Journal of Thermal Analysis and Calorimetry (2021) 143:3643–3654
https://doi.org/10.1007/s10973-019-09223-3

Effectiveness of Cattaneo–Christov double diffusion in Sisko fluid flow with variable properties: Dual solutions

Latif Ahmad[1,2] · Jawad Ahmed[1,3] · Masood Khan[1] · Muhammad Yasir[1] · Metib Alghamdi[4]

Received: 3 August 2019 / Accepted: 19 December 2019 / Published online: 25 January 2020

Abstract

The nature and properties of generalized Newtonian fluid flows are of the most significant phenomena applicable to engineering applications. But this particular portion of research work incorporates the importance of flow, heat and mass transfer analysis of non-homogeneous Sisko fluid transport model. The flow source in this study is assumed by the stretching and shrinking velocities of the sheet. Therefore, the influence of these two velocities creates a phenomenon of multiple solutions. The effect of magnetic field is another significant physical parameter in the flow analysis and has been considered in this study. Moreover, the impacts of variable thermal conductivity, mass diffusivity and suction/injection are also incorporated. The system of conservative governing partial differential equations are converted into a dimensionless system of equations by using the suitable transformations. The new system of equations along with the corresponding transformed boundary conditions are then solved numerically with the help of collocation method in Matlab. This method is a built-in approach for the solution of nonlinear boundary value problem. In comparison with other user-defined numerical approaches, this method is little bit fast and works accurately because this method uses finite difference method for modifying weak initial guess and the CPU timing is very small as compared to other built-in approaches. The present results are shown for the existence of multiple (upper branch and lower branch) solutions for a specific range of involved physical parameters. The critical values of shrinking parameter corresponding to suction parameter and Sisko fluid parameter are computed in the certain range of ($\chi_c < \chi < 0$). The behaviors of various dimensionless parameters on different profiles are discussed graphically. The increase in material parameter causes a reduction in skin friction for both cases, i.e., shear-thinning as well as shear-thickening fluids. The first and second solutions of temperature and concentration profiles, respectively, show increasing and decreasing trends for an increase in temperature and concentration time relaxation parameters.

Keywords Generalized Newtonian fluids · Shrinking surface · Variable thermal conductivity · Mass diffusivity: multiple solutions

List of symbols

A	Material parameter of Sisko fluid
B_0	Magnetic field strength (A/m)
$B(x)$	Variable magnetic field
c	Constant
C_w	Wall species concentration ($\mathrm{kg\,m^{-3}}$)
C_∞	Ambient concentration, ($\mathrm{kg\,m^{-3}}$)
D	Mass diffusivity ($\mathrm{m^2\,s^{-1}}$)
f	Dimensionless stream function
k	Thermal conductivity ($\mathrm{W\,m^{-1}\,K^{-1}}$)
M	Dimensionless magnetic parameter
n	Non-Newtonian power-law index
η	Similarity variable
μ	Dynamic viscosity ($\mathrm{Ns\,m^{-2}}$)
υ	Kinematic viscosity ($\mathrm{m^2\,s^{-1}}$)
λ_E	Thermal relaxation parameter
λ_C	Thermal concentration parameter
ε_1	Variable thermal conductivity
ε_2	Variable mass diffusivity
Pr	Prandtl number
s	Nonlinear stretching parameter

✉ Jawad Ahmed
jawad.ahmed@uettaxila.edu.pk

1 Department of Mathematics, Quaid-i-Azam University, Islamabad 44000, Pakistan

2 Department of Mathematics, Shaheed Benazir Bhutto University, Sheringal, Dir Upper 18000, Pakistan

3 Department of Basic Sciences, University of Engineering and Technology, Taxila 47050, Pakistan

4 Department of Mathematics, Faculty of Science, King Khalid University, Abha 61413, Saudi Arabia

S	Mass transfer parameter
Sc	Schmidt number
T_w	Wall temperature (K)
T_∞	Ambient fluid temperature (K)
u, v	Velocity components (m s^{-1})
u_w	Velocity of sheet (m s^{-1})
v_w	Mass transfer velocity (m s^{-1})
x, y	Cartesian coordinates (m)
σ	Electric conductivity of base fluid (S m^{-1})
τ_w	Shear stress at surface (N m^{-2})
$(\rho c)_f$	Heat capacity of base fluid (J K^{-1})
χ	Stretching/shrinking parameter
θ	Dimensionless temperature
ϕ	Dimensionless concentration
f'	Dimensionless velocity

Introduction

The phenomenon of fluid flow plays a vital role in various industrial and engineering applications [1–17]. A wide range of applications of heat and the mass transfer analysis due to flow of non-Newtonian fluids can be observed, such as petroleum reservoirs, heat exchangers, material process system. The non-Newtonian fluids are abundant in various involved industrial applications and heat transfer processes as compared to Newtonian fluids. The equation for the non-Newtonian fluids does not execute the linear connection across the shear stress and strain rate. The flow and heat transfer analysis of these fluids has been explained by various researchers with different physical situations.

In perspective on numerous such applications, Sheikholeslami et al. [18] commence the analytical study on MHD free convection of nanofluid considering the impacts of thermal radiation with a stretching sheet. Prasannakumara et al. [19] studied that in the case of nonlinear stretching sheet the Nusselt number and Sherwood number are higher with the effect of magnetic field on nanofluid radiative heat transfer. Sheikholeslami and Ellahi [20] investigated that the rise of Lorentz forces detracts the convection in a cubic cavity. MHD viscous flow due to a shrinking sheet has been done by Sajid and Hayat [21]. Hsiao [22] investigated the effects of stagnation-point flow on MHD nanofluid mixed convection with the existence of boundary slip on stretching sheet. Cortell [23] indicates that the magnetohydrodynamic flow and a nonlinear radiative heat transfer of a viscoelastic fluid over a stretching sheet with the generation/absorption of heat at energy aspect. The articles discussed by Sheikholeslami [15, 24–29] revealed the significant importance of magnetic field. Subsequently, many researchers extended this kind of work to Newtonian/non-Newtonian boundary layers flow with assorted velocity and the thermal boundary condition. In view of such extensive materials, many authors have made efforts to illustrate the analysis of flow and heat with non-Newtonian fluids along with a Sisko fluid model [30–33].

The above referred works concern the consistent physical properties of a cooling fluid, but in practical situations the physical properties are needed with variable characteristics. That is why the one such property is a thermal conductivity, which is considered to vary linearly with a temperature. The heat transfer analysis in a viscous fluids flow over a permeable surface along with temperature field is presented by Mahmood et al. [34]. Salahuddin et al. [35], using the Keller box method, discussed the combined impacts of variable thermal conductivity and the MHD flow on pseudoplastic fluid. Abel et al. [36] deliberated the effects of variable thermal conductivity in a power-law fluid past a stretching surface in the existence of non-uniform heat source. Recently, Malik et al. [37, 38] have initiated the flow of non-Newtonian fluids over a stretching cylinder and heat transfer with viscous dissipation and variable thermal conductivity. In one of these investigations, the physical properties of the fluids were thought to be consistent. Although it is notable that such properties increase or decrease with the temperature. Consequently, the related articles [39–44] demonstrate that this sort of flow has not been explored for power-law fluids within the sight of stretching sheet. Zhang et al. [45] presented another model on the temperature field by considering the impacts of power law, they expected that the temperature field is same as velocity field, while the thermal diffusivity shifts as a component of temperature slope. Yu and Choi [46] altered the Maxwell's equation and the Hamilton's Crosser relation for the effective thermal conductivity to incorporate the impact of requested nano-layers surrounding the particles. Jang and Choi [47] proposed a powerful thermal conductivity model by considering the impacts of Brownian motion particles. They concentrated on the heat transfer among particles and the carrier fluid, ignoring the blending because of irregular molecule movement.

Furthermore, some researchers focus on the combining investigation of non-Newtonian fluids with the convection process. A numerical studied on such types of heat transfer execution of nanofluids over a porous stretching sheet is exhibited by Das [48]. Huang et al. [49] also discussed the unsteady flow with a heat transfer enclosure held on a circular cylinder. Convection flow based on boundary layer from a circular cylinder with uniform surface heat flux transfer is explored by Bhowmick et al. [50].

All the overhead examinations were carried out for fluids having magnetic field, variable thermal conductivity and the mass diffusivity, right through the flow regime. Although it is realized that the physical properties change with the temperature, the effects of these quantities on the heat transfer have become more useful in engineering and applications process such as crude oil extraction, geothermal systems and ground water pollution. The main purpose of the current work is to study the dual nature of magnetohydrodynamics flow with the heat and mass transfer analysis embedded in permeable media under the impacts of thermal conductivity and the mass diffusivity. The governing PDEs have been solved by using bvp4c techniques in Matlab.

Mathematical formulation

Here, we consider the steady, laminar and incompressible two-dimensional flow of a Sisko fluid originate by semi-infinite shrinking surface with the velocity $u_{\mathrm{w}} = cx^{s}$, in the region upper half plane. The velocity v_{w} on the wall is perpendicular to the sheet. Further, it is assumed that the velocity $v = v_0$ is the constant mass flux velocity which is taken to be positive in the case of suction while taking negative in the case of blowing on the sheet along the axial direction. In the positive y-direction, a uniform transverse magnetic field $\left(B_0 x^{(s-1)/2}\right)$ is applied normal to the stretching surface. And the effects of thermal conductivity and mass diffusivity are also considered. Moreover, T_{w} and C_{w} represent the temperature and the concentration at the wall surface of shrinking sheet, while T_∞ the temperature and C_∞ the concentration at the ambient surface such that ($T_\infty < T_{\mathrm{w}}$) and ($C_\infty < C_{\mathrm{w}}$). In this analysis, we considered the positive velocity gradient due to the boundary layer approximation the flow is over the shrinking surface (Fig. 1).

For the Sisko fluid model, the extra stress tensor is [51]:

$$\mathbf{S} = \left\{ a + b \left| \sqrt{\frac{1}{2} tr\left(\mathbf{A}_1\right)^2} \right|^{n-1} \right\} \mathbf{A}_1, \tag{1}$$

with

$$\mathbf{A}_1 = \nabla \mathbf{V} + (\nabla \mathbf{V})^{\mathrm{T}}. \tag{2}$$

By using the above suppositions, the model equations are governed into the following form:

$$\frac{\partial u}{\partial x} + \frac{\partial v}{\partial y} = 0, \tag{3}$$

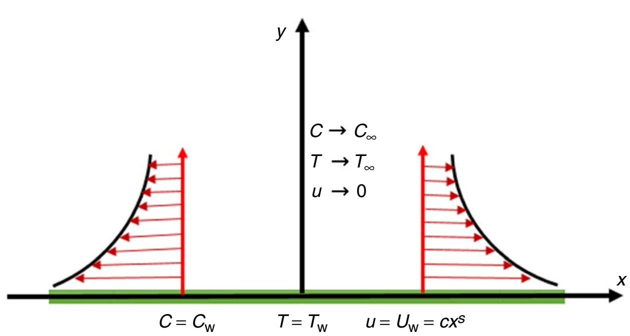

Fig. 1 Physical geometry and coordinates system

$$u\frac{\partial u}{\partial x} + v\frac{\partial u}{\partial y} = \frac{a}{\rho_{\mathrm{f}}}\left(\frac{\partial^2 u}{\partial y^2}\right) + \frac{b}{\rho_{\mathrm{f}}}\frac{\partial}{\partial y}\left(\frac{\partial u}{\partial y}\right)^{\mathrm{n}} - \frac{\sigma B_0^2}{\rho_{\mathrm{f}}}u, \tag{4}$$

$$u\frac{\partial T}{\partial x} + v\frac{\partial T}{\partial y} + \delta_{\mathrm{E}}\begin{bmatrix} u^2\frac{\partial^2 T}{\partial x^2} + 2uv\frac{\partial^2 T}{\partial x \partial y} + v^2\frac{\partial^2 T}{\partial y^2} \\ +\left(u\frac{\partial u}{\partial x} + v\frac{\partial u}{\partial y}\right)\frac{\partial T}{\partial x} \\ +\left(u\frac{\partial v}{\partial x} + v\frac{\partial v}{\partial y}\right)\frac{\partial T}{\partial y} \end{bmatrix} = \frac{1}{\rho c_{\mathrm{f}}}\frac{\partial}{\partial y}\left(k(T)\frac{\partial T}{\partial y}\right), \tag{5}$$

$$u\frac{\partial C}{\partial x} + v\frac{\partial C}{\partial y} + \delta_{C}\begin{bmatrix} u^2\frac{\partial^2 C}{\partial x^2} + 2uv\frac{\partial^2 C}{\partial x \partial y} + v^2\frac{\partial^2 C}{\partial y^2} \\ +\left(u\frac{\partial u}{\partial x} + v\frac{\partial u}{\partial y}\right)\frac{\partial C}{\partial x} \\ +\left(u\frac{\partial v}{\partial x} + v\frac{\partial v}{\partial y}\right)\frac{\partial C}{\partial y} \end{bmatrix} = \frac{\partial}{\partial y}\left(D(C)\frac{\partial C}{\partial y}\right), \tag{6}$$

the BC's are

$$\begin{aligned} u &= \chi u_{\mathrm{w}}(x), v = v_{\mathrm{w}}(x), T = T_{\mathrm{w}}, C = C_{\mathrm{w}} \text{ at } y = 0, \\ u &= 0, v = 0, T = T_\infty, C = C_\infty \text{ as } y \to \infty, \end{aligned} \tag{7}$$

where u and v denote the velocity components in x- and y-directions, respectively, σ is the electrical conductivity, p is a fluid pressure, T denotes the fluid temperature and C the fluid concentration, respectively, ρ_{f} a fluid density and c_{f} the specific heat, and χ is shrinking ($\chi < 0$) / stretching ($\chi > 0$) parameter. Introducing a stream function $\psi(x, y)$

$$u = \frac{\partial \psi}{\partial y} \text{ and } v = -\frac{\partial \psi}{\partial x},$$

where $\psi(x, y) = u_{\mathrm{w}} x \mathrm{Re}_{\mathrm{b}}^{-\frac{1}{n+1}} f(\eta)$, with $f(\eta)$ is a dimensionless stream function where $\eta = \frac{y}{x}\mathrm{Re}_{\mathrm{b}}^{\frac{1}{n+1}}$. Thus,

$$u = u_{\mathrm{w}} f'(\eta), v = -u_{\mathrm{w}}\mathrm{Re}_{\mathrm{b}}^{-\frac{1}{n+1}}\left[\left\{\frac{s(2-n)-1}{1+n}\right\}\eta f'(\eta) + \left\{\frac{s(2n-1)+1}{1+n}\right\}f(\eta)\right], \tag{8}$$

$$\theta(\eta) = \frac{T - T_\infty}{T_{\mathrm{w}} - T_\infty}, \quad \phi(\eta) = \frac{C - C_\infty}{C_{\mathrm{w}} - C_\infty}, \tag{9}$$

where $\theta(\eta)$ and $\phi(\eta)$ are the dimensionless temperature and concentration for the fluid. By using Eqs. (8) and (9) , Eqs. (3) to (6) transform into the following set of nonlinear ODEs as:

$$\left(A + n(f'')^{\mathrm{n}-1}\right)f''' - sf'^2 + \left\{\frac{s(2n-1)+1}{1+n}\right\}ff'' - Mf' = 0, \tag{10}$$

$$(1+\varepsilon_1\theta)\theta'' + \varepsilon_1\theta'^2 + \Pr\left\{\frac{s(2n-1)+1}{1+n}\right\}f\theta' - \Pr\lambda_E\left\{\frac{s(2n-1)+1}{1+n}\right\} \times \left[\{2+n+(n-2)s\}ff'\theta' + \{s(2n-1)+1\}f^2\theta''\right] = 0, \tag{11}$$

$$(1+\varepsilon_2\phi)\phi'' + \varepsilon_2\phi'^2 + \mathrm{Sc}\left\{\frac{s(2n-1)+1}{1+n}\right\}f\phi' - \mathrm{Sc}\lambda_C\left\{\frac{s(2n-1)+1}{1+n}\right\} \times \left[\{2+n+(n-2)s\}ff'\phi' + \{s(2n-1)+1\}f^2\phi''\right] = 0, \tag{12}$$

and the BC's become

$$\begin{aligned} &f(\eta) = S,\ f'(\eta) = \chi, \theta(\eta) = 1, \phi(\eta) = 1 \text{ at } \eta = 0,\\ &f'(\eta) = 0,\ \theta(\eta) = 0,\ \phi(\eta) = 0 \text{ as } \eta \to \infty, \end{aligned} \tag{13}$$

where $\mathrm{Re_a}\left(=\frac{\rho x u_w}{a}\right)$, and $\mathrm{Re_b}\left(=\frac{\rho x^n u_w^{2-n}}{b}\right)$ are the Reynolds numbers, $A\left(=\frac{\mathrm{Re_b}^{\frac{2}{n+1}}}{\mathrm{Re_a}}\right)$ denotes the material parameter, $M\left(=\frac{\sigma B_0^2}{a\rho}\right)$ is a magnetic field parameter, $\lambda_{E,C}\left(=\frac{u_w\delta_{E,C}}{x}\right)$ is a relaxation parameters, $\Pr\left(=\frac{xu_w}{a}\mathrm{Re_b}^{\frac{-2}{n+1}}\right)$ represents the generalized Prandtl number and $\mathrm{Sc}\left(=\frac{xu_w\mathrm{Re_b}^{\frac{-2}{n+1}}}{D}\right)$ is the generalized Schmidt numbers, and $S\left(=-\frac{\upsilon_w}{\left(\frac{s(2n-1)+1}{n+1}\right)u_w\mathrm{Re_b}^{\frac{-2}{n+1}}}\right)$ is the suction parameter.

From Eq. (10), it tends to be seen that for $A=0$ and distinct values of a power-law index, different kinds of fluid behaviors are recovered. For $n=1$, the behavior of the fluid is Newtonian and for $n \neq 1$ the behavior of the fluid is non-Newtonian ($n>1$ shear thickening and $n<1$ shear thinning). Also when $n=1$, we have $\mathrm{Re_a} = \mathrm{Re_b}$ which represents the global similarity. The physical attributes of C_f is described as

$$C_f = \frac{\tau_w}{\rho u_w^2}, \tag{14}$$

where the shear stress τ_w is defined as

$$\tau_w = \left[a\left(\frac{\partial u}{\partial y}\right) + b\left(\frac{\partial u}{\partial y}\right)^n\right]_{y=0}. \tag{15}$$

In dimensionless notation, the quantity skin friction becomes

$$C_f\mathrm{Re_b}^{\frac{-1}{n+1}} = Af''(0) + \left[f''(0)\right]^n. \tag{16}$$

Solution methodology

The non-dimensional governing equations of the model problem are nonlinear PDEs in nature. Thus, to solve this system we first transform these into a new dimensionless form of ODEs along with boundary conditions depending on a single variable η. For further solving, we go toward numerical simulation. Therefore, the transformed governing ODEs in Eqs. (10–12) with conditions (13) are numerically integrated by using the bvp4c in Matlab. In utilizing this technique, the dimensionless system of equations are initially reduced into the set of first-order differential equations by familiarizing with some new variables given by

$$f = y_1,\ f' = y_2, f'' = y_3, \theta = y_4, \theta' = y_5, \phi = y_6, \phi' = y_7. \tag{17}$$

Therefore, the reduced system of first-order equations is

$$\begin{pmatrix} y_1' \\ y_2' \\ y_3' \\ y_4' \\ y_5' \\ y_6' \\ y_7' \end{pmatrix} = \begin{pmatrix} y_2 \\ y_3 \\ \dfrac{sf'^2 - \left(\frac{s(2n-1)+1}{n+1}\right)ff'' + M^2 f'}{A + n(f'')^{n-1}} \\ y_5 \\ \dfrac{\Pr\lambda_E\left(\frac{s(2n-1)+1}{(n+1)^2}\right)\times\{2+n+(n-2)s\}ff'\theta' - \Pr\left(\frac{s(2n-1)+1}{n+1}\right)f\theta' - \varepsilon_1\theta'^2}{1+\varepsilon_1\theta - \Pr\lambda_E\left(\frac{s(2n-1)+1}{(n+1)^2}\right)\times\{s(2n-1)+1\}f^2} \\ y_7 \\ \dfrac{\mathrm{Sc}\lambda_C\left(\frac{s(2n-1)+1}{(n+1)^2}\right)\times\{2+n+(n-2)s\}ff'\phi' - \mathrm{Sc}\left(\frac{s(2n-1)+1}{n+1}\right)f\phi' - \varepsilon_2\phi'^2}{1+\varepsilon_2\phi - \mathrm{Sc}\lambda_C\left(\frac{s(2n-1)+1}{(n+1)^2}\right)\times\{s(2n-1)+1\}f^2} \end{pmatrix}, \tag{18}$$

with conditions

$$\begin{aligned} &y_1(0) = S,\ y_2(0) = \chi,\ y_2(\infty) = 0,\ y_4(0) = 1,\\ &\quad y_4(\infty) = 0,\ y_6(0) = 1,\ y_6(\infty) = 0. \end{aligned} \tag{19}$$

Flow, heat and mass transfer problem of Sisko fluid is considered for testing the influence of various flow parameters with the help of numerical approach. In particular, all these effects are summarized in the form of first and second approximated values of local skin friction, Nusselt number and Sherwood number. However, these results are well correlated with results presented by Bhattacharyya [34] and Ishak et al. [35] as illustrated in Table 1.

Graphical results and discussion

Numerical solutions to the ordinary differential equations (10) to (12) along with the boundary conditions (13) were obtained by using one of the collocation methods in Matlab. In this techniques, the multiple solutions are obtained by setting different initial guesses for the values of $f''(0)$, $\theta'(0)$ and $\phi(0)$, where all profiles satisfy the boundary conditions asymptotically with different boundary layer thickness. The actual domain is infinite but the results concluded for finite domain because the software is working only for finite value of domain.

The variation of $f''(0)$ with shrinking parameter χ for shear-thinning fluid in panel (a) and shear-thickening fluid in panel (b) is shown in Fig. 2 and Fig. 3 for the representative values of Sisko fluid parameter and mass suction parameter, respectively. These figures show that there is a region of single solution for $\chi \geqslant -1$, dual (upper branch and lower branch) solutions for $\left(\chi_c < \chi < -1\right)$ and there are no solutions for $\left(\chi < \chi_c\right)$. Here, χ_c represent the critical values (turning points) of χ that depend on A and S.

Figure 2 displays the impacts of skin friction for the surface of Sisko fluid parameter A for distant values of the shrinking parameter χ. In shear-thinning fluid critical values are changing from $\chi_c = -1.5065$ to $\chi_c = -1.6360$, whereas in shear-thickening fluid critical values decrease from $\chi_c = -2.3804$ to $\chi_c = -3.4054$. Here, we also noted that the dual-nature solutions of skin friction are reduced with increasing the values of $A = \{3, 4, 5\}$ and $\{50\%,\ 60\%, 83\%\}$ in percentage term.

Also, Fig. 3 depicts the evaluation for numerous values of mass suction parameter ($S > 0$); the skin friction is sketched with reference to shrinking parameter χ. We noted that the critical values for shear-thinning fluid are decreasing from $\chi_c = -2.2846$ to $\chi_c = -2.6296$, whereas in shear-thickening fluid critical values are decreasing from $\chi_c = -4.0094$ to $\chi_c = -4.4094$. Thus, skin friction rises with rising the variation of $S = \{3.0, 3.1, 3.2\}$and $\{75\%, 77.5\%,\ 80\%\}$ in percentage term. Also we noted that multiple solutions of skin friction are higher for A as compared to the S.

The profile $f'(\eta)$ for the several values of Sisko fluid parameter A is shown in Fig. 4 with the first solution being shown by a full line and the second solutions by a broken line. It is depicted that the fluid velocity distribution decreases in the upper branch solution and increases in the lower branch solution, while in the case of shear thickening, the upper branch solution and the lower branch solution are showing a decreasing pattern. Also, the thickness of a momentum boundary layer increases with this effect.

Figure 5 shows the impacts of S on $f'(\eta)$. It is perceived that the impact of suction parameter S has the opposite trend in upper branch and lower branch solutions, *i.e.*, the strong influence of S causes the fluid velocity to increase in upper branch, while it causes the fluid velocity to decrease in the lower branch. Furthermore, the behavior of the boundary layer of the flow can also be analyzed through these figures. Thus, we observed that the related thickness is declined and is raised in the upper branch and lower branch solutions, respectively, with the increasing value of $S = \{3.0, 3.4, 3.8\}$ and $\{75\%, 85\%,\ 95\%\}$ in percentage term.

Figure 6 shows the prominent attributes of shrinking parameter χ on fluid velocity against the dimensionless parameter η. For both the cases, the velocity increases with increasing the magnitude of χ for the first branch, whereas opposite behavior is seen in the second branch. Consequently, the momentum boundary layer thickness is showing reduction in the upper branch case, while the reverse is true for the lower branch.

Figure 7 reveals the magnetic field effects on the momentum boundary layer. By analyzing these graphs, it is elucidated that the strong magnetic field improves the boundary layer in the upper branch, while it conflicts in the lower branch solution. Also we noted that due to the effect of Lorentz forces the magnitudes of the first velocity profile are lower with the variation of M and that the motion of the fluid is declined. On the other way, the velocity profile is not realizable physically; that is why in a physical situation the

Table 1 Comparison of $f''(0)$ for first and second solutions with different values of shrinking parameter χ by keeping $n = s = 1$, when the other parameters are zero

	Bhattacharyya. [52]		Ishak et al. [53]		Present results	
χ	First	Second	First	Second	First	Second
− 0.50	1.4956697		1.495670		1.4951062	
− 0.75	1.4892981		1.489298		1.4895589	
− 1.00	1.3288169	0	1.328817	0	1.3286050	0
− 1.15	1.0822316	0.1167023	1.082231	0.116702	1.0820049	0.1167059
− 1.20	0.9324728	0.2336491	0.932474	0.233650	0.9304351	0.2336011
− 1.2465	0.5842915	0.5542856	0.584295	0.554283	0.5841111	0.5546414

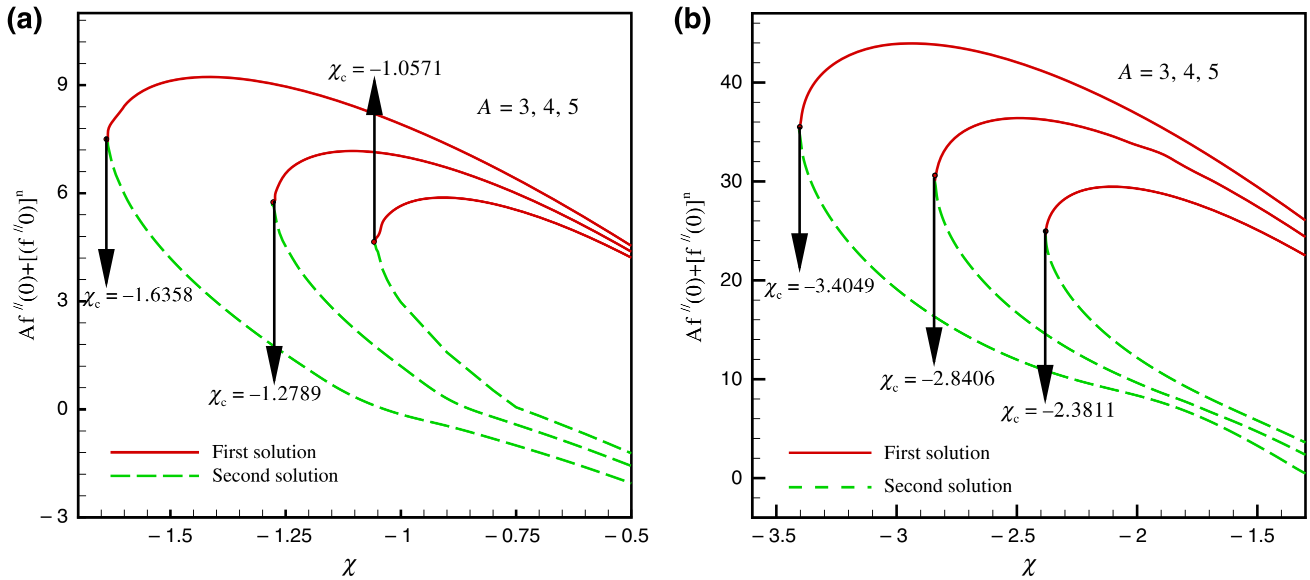

Fig. 2 The impact of Sisko fluid parameter A on skin friction coefficient with shrinking parameter χ

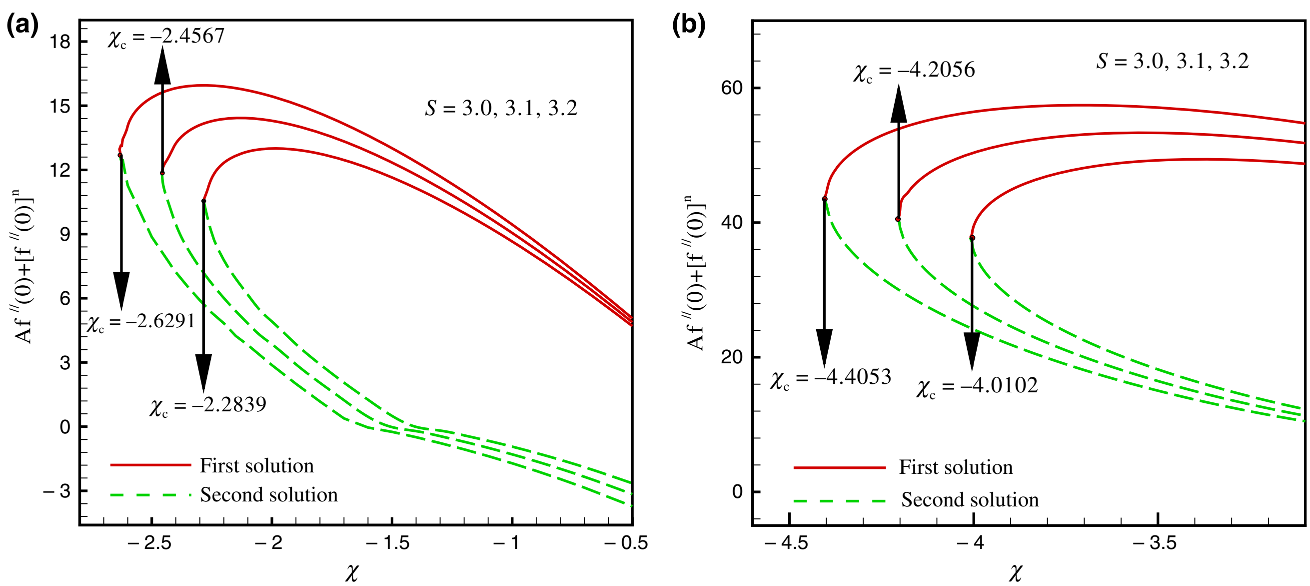

Fig. 3 The variation of skin friction at the surface with shrinking parameter (χ) for distant values of mass suction parameter (S).

second solution is unstable. Here, we vary the value of M in percentage term as $\{10\%, 25\%, 40\%\}$.

The impact of Pr on dimensionless temperature distribution $\theta(\eta)$ is shown in Fig. 8a. The percent values of Pr are increased in a manner $\{32\%, 33\%, 35\%\}$ depending upon the convergence region of Pr. An increase in Pr physically implies a reduction of fluid thermal conductivity; thus, the decline is seen in the thickness of a thermal boundary layer.

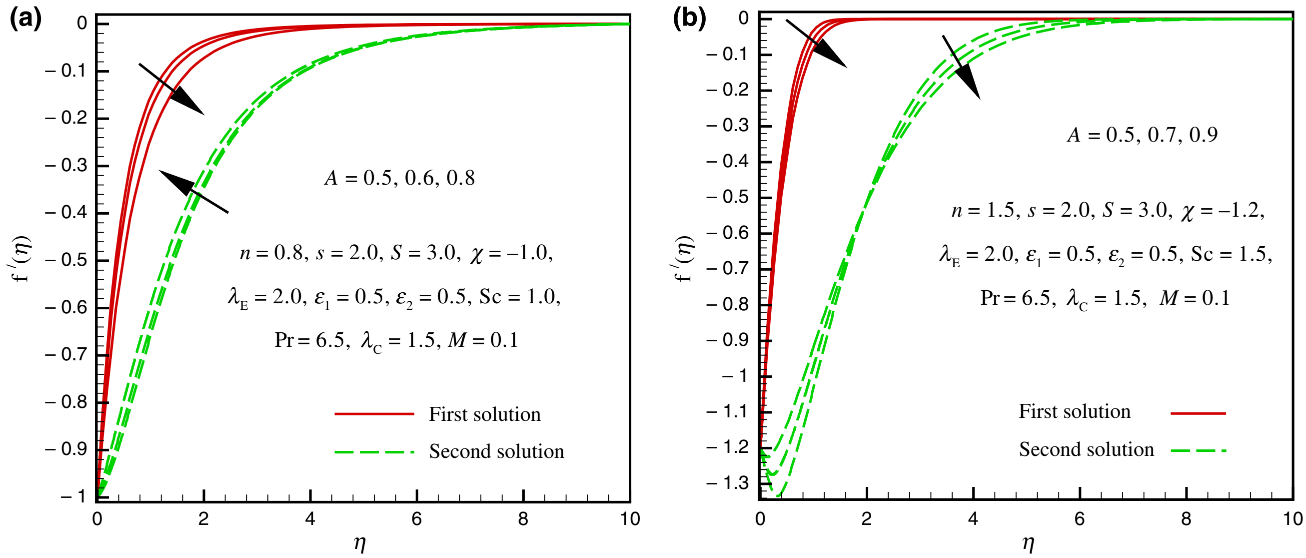

Fig. 4 The dual behavior of $f'(\eta)$ with the variation of A

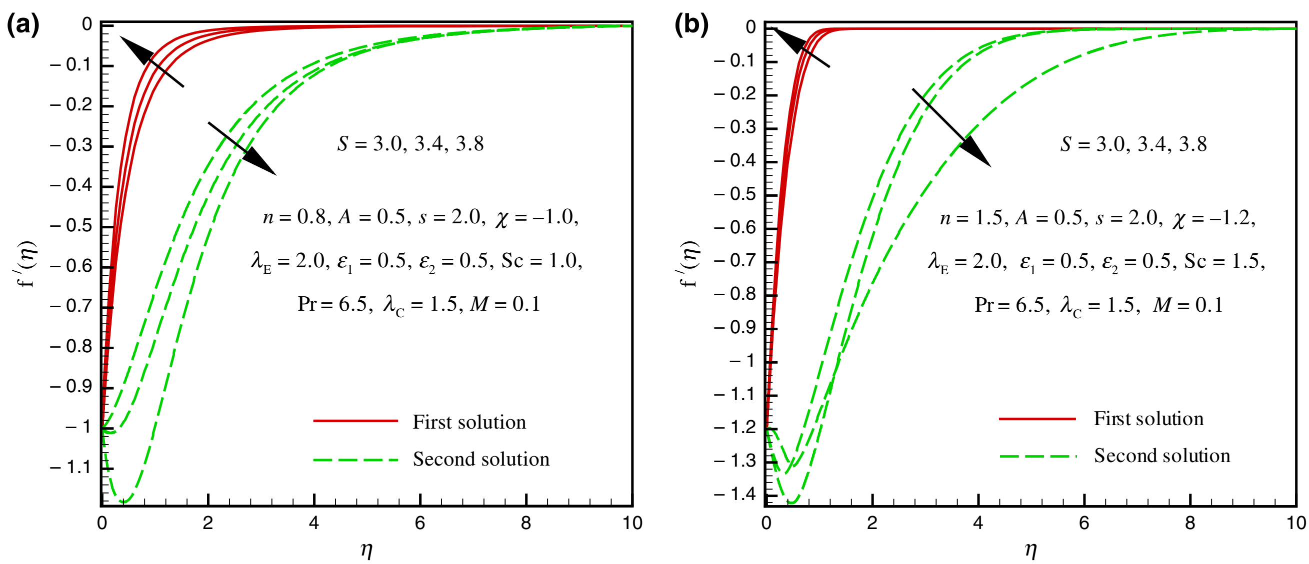

Fig. 5 The dual behavior of $f'(\eta)$ with the variation of S

Also, the temperature profile is showing a decreasing behavior in the first branch and increasing one in second branch solution with increasing values of Pr. So there is no effect of Pr on the velocity fluid because the momentum equation is independent of the thermal one. Furthermore, from Fig. 8b we noted that as we increased the values of λ_E, the fluid temperature and the thickness of the related boundary layers diminished. Physically, this is due to the reality that the liquid particle needs enough time to transport the heat to its nearest particles. Additionally, for the larger values

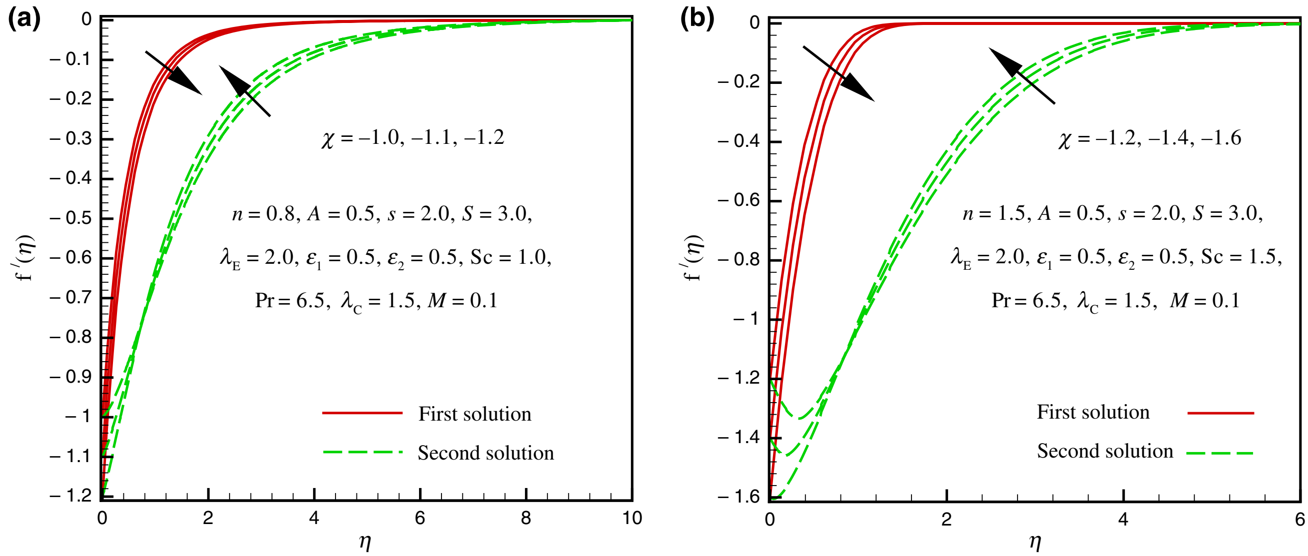

Fig. 6 The dual behavior of $f'(\eta)$ with the variation of χ

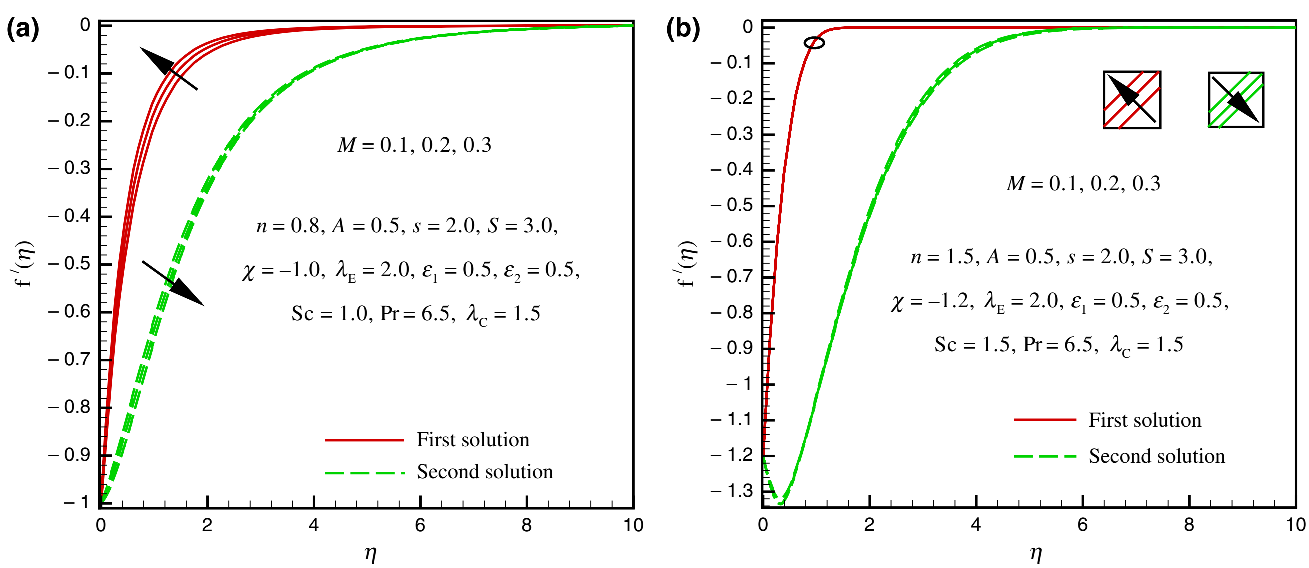

Fig. 7 The dual behavior of $f'(\eta)$ with the variation of M

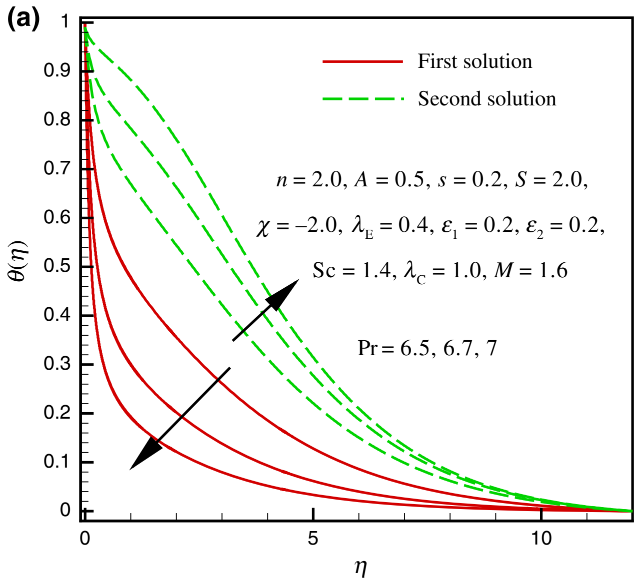

Fig. 8 The dual behavior of $\theta(\eta)$ with the variation of Pr in (panel-a) and λ_E in (panel-b)

of λ_E the conduct of liquid as a non-conductor which is in charge of the decrease of $\theta(\eta)$ (Fig. 9). The fluctuation in the temperature distribution and the related boundary layer thickness for the ϵ_1 is shown in Fig. 10. It is concluded from the figure that the fluid temperature shows an increasing behavior with the enlargement of ϵ_1 in upper branch and lower branch solutions, which is a result of the way that the thermal conductivity improves the temperature.

The variation of Sc and λ_c on concentration profile is shown in Fig. 10a,b. Schmidt number Sc causes the concentration profile to minimize in the first solution as well as in the second solution. The enhancment in Schmidt number decreases the concentration distribution as well as the associated boundary layer thickness and this is due to an inverse relation of Schmidt number with molecular diffusivity. So, concentration distribution and concentration boundary layer thickness diminished. The corresponding dual dimensionless concentration profiles are shown in Fig. 9b. For the second solution, the peak of the concentration overshoot increases with increasing concentration relaxation parameter and the thickness of a concentration boundary layer is always greater

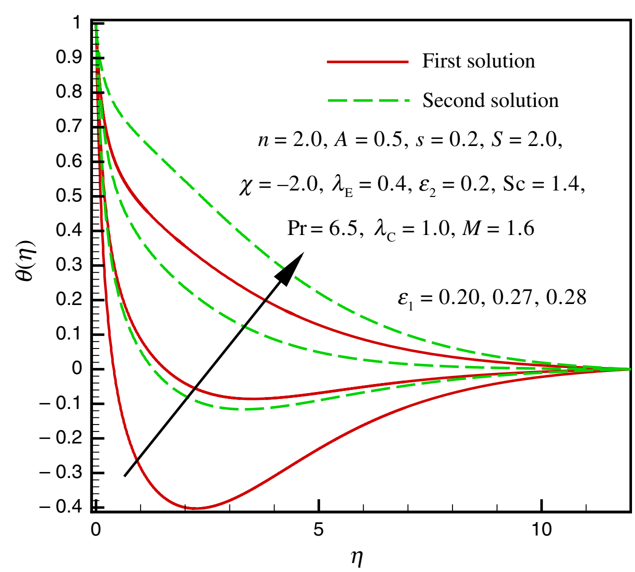

Fig. 9 The dual behavior of $\theta(\eta)$ with the variation of ϵ_1

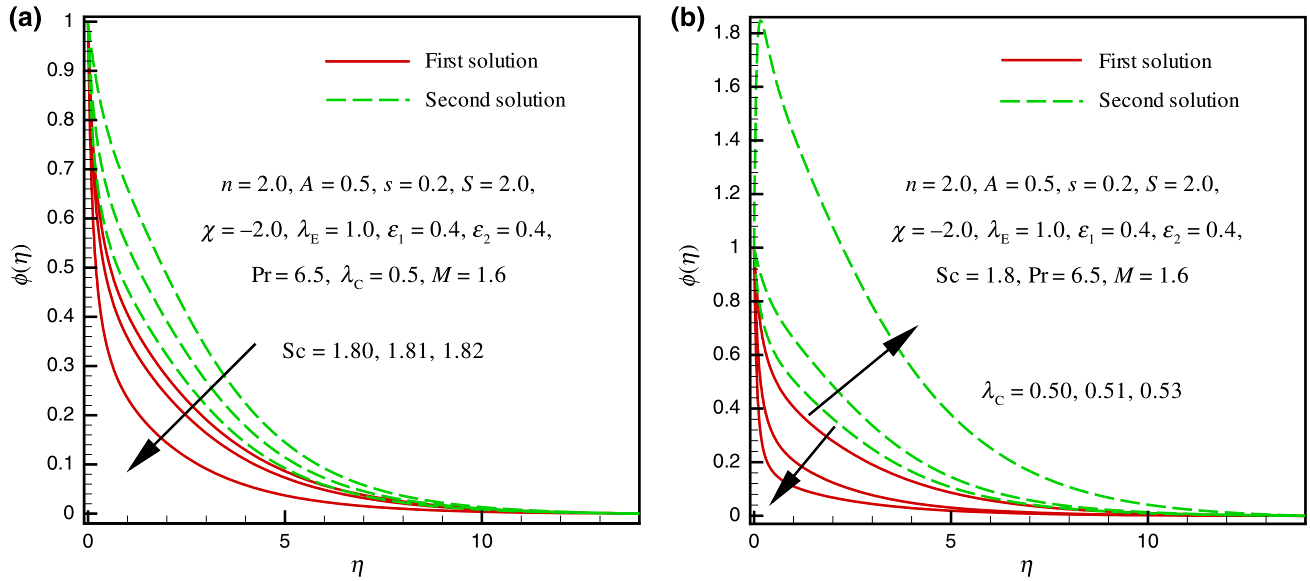

Fig. 10 The dual behavior of $\phi(\eta)$ with the variation of **a** Sc **b** λ_C

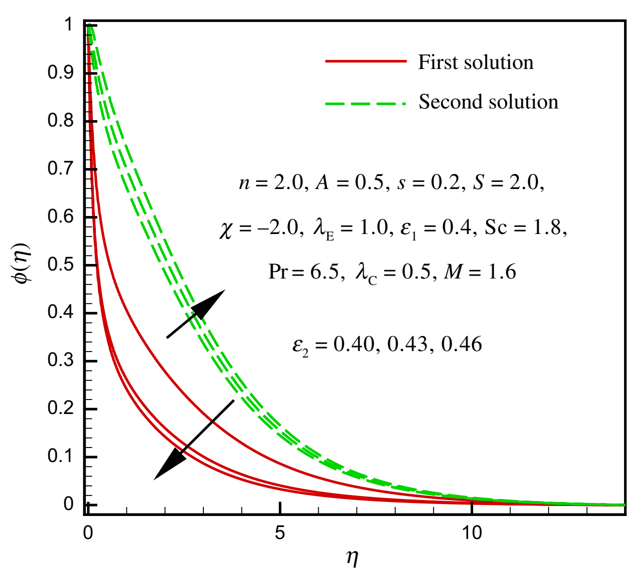

Fig. 11 The dual behavior of $\phi(\eta)$ with the variation of ϵ_2

than that of the first solution. Figure 11 displays the concentration profile for distant values of ϵ_2. As we see from the figure, the related thickness for the first solution is greater than for the second solution. The concentration profile declines with the variation of ϵ_2 for the first solution, however increment for the second solution.

Conclusions

A numerical simulation is employed to examine the dual-nature solutions for the MHD Sisko fluid flow over a uniformly shrinking sheet. In this work, magnetic field and suction effects were taken into the account for the fluid flow and heat transfer analysis. The results were obtained for the multiple (upper branch and lower branch) solutions of modeled problem by utilizing the Matlab built-in function, namely bvp4c. On the basis of the present work, we have concluded some remarkable features as follows:

- The upper solution is physically stable, whereas the lower solution is unstable.
- The more suction S into the Sisko fluid flow increases the fluid velocity in upper branch, while it reduces in the lower branch.
- The thickness of momentum and thermal boundary layer are thinner in upper branch compared with the lower branch.
- Temperature fluid rises with rising the values of variable thermal conductivity.

Acknowledgements The authors extend their appreciation to the Deanship of Scientific Research at King Khalid University, Saudi Arabia, for funding this work through Research Groups Program under Grant number (RGP2/26/40).

References

1. Sun F, Yao Y, Li X, Yu P, Zhao L, Zhang Y. A numerical approach for obtaining type curves of superheated multi-component thermal fluid flow in concentric dual-tubing wells. Int J Heat Mass Transf. 2017;111:41–53.
2. Sun F, Yao Y, Chen M, Li X, Zhao L, Meng Y, Sun Z, Zhang T, Feng D. Performance analysis of superheated steam injection for heavy oil recovery and modeling of wellbore heat efficiency. Energy. 2017;125:795–804.
3. Sun F, Yao Y, Li X, Tian J, Zhu G, Chen Z. The flow and heat transfer characteristics of superheated steam in concentric dual-tubing wells. Int J Heat Mass Transf. 2017;115(Part B):1099–108.
4. Zhao C, Qiao X, Cao Y, Shao Q. Application of hydrogen peroxide presoaking prior to ammonia fiber expansion pretreatment of energy crops. Fuel. 2017;205:184–91.
5. Sun F, Yao Y, Li X, Zhao L. Type curve analysis of superheated steam flow in offshore horizontal wells. Int J Heat Mass Transf. 2017;113:850–60.
6. Sun F, Yao Y, Li X, Zhao L, Ding G, Zhang X. The mass and heat transfer characteristics of superheated steam coupled with non-condensing gases in perforated horizontal wellbores. J Petrol Sci Eng. 2017;156:460–7.
7. Sun F, Yao Y, Li X, Yu P, Ding G, Zou M. The flow and heat transfer characteristics of superheated steam in offshore wells and analysis of superheated steam performance. Comput Chem Eng. 2017;100:80–93.
8. Sun F, Yao Y, Li G, Li X. Geothermal energy development by circulating CO_2 in a U-shaped closed loop geothermal system. Energy Conver Manag. 2018;174:971–82.
9. Sun F, Yao Y, Li G, Li X. Performance of geothermal energy extraction in a horizontal well by using CO_2 as the working fluid. Energy Conver Manag. 2018;171:1529–39.
10. Sun F, Yao Y, Li G, Li X. Geothermal energy extraction in CO_2 rich basin using abandoned horizontal wells. Energy. 2018;158:760–73.
11. Sun F, Yao Y, Li X. The heat and mass transfer characteristics of superheated steam coupled with non-condensing gases in horizontal wells with multi-point injection technique. Energy. 2018;143:995–1005.
12. Qiao X, Zhao C, Shao Q, Hassan M. Structural characterization of corn stover lignin after hydrogen peroxide presoaking prior to ammonia fiber expansion pretreatment. Energy Fuels. 2018;32:6022–30.
13. Sheikholeslami M, Jafaryar M, Saleem S, Li Z, Shafee A, Jiang Y. Nanofluid heat transfer augmentation and exergy loss inside a pipe equipped with innovative turbulators. Int J Heat Mass Transf. 2018;126:156–63.
14. Sheikholeslami M, Ghasemi A, Li Z, Shafee A, Saleem S. Influence of CuO nanoparticles on heat transfer behavior of PCM in solidification process considering radiative source term. Int J Heat Mass Transf. 2018;126:1252–64.
15. Sheikholeslami M, Shehzad SA. CVFEM simulation for nanofluid migration in a porous medium using Darcy model. Int J Heat Mass Transf. 2018;122:1264–71.
16. Sheikholeslami M, Arabkoohsar A, Jafaryar M. Impact of a helical-twisting device on the thermal-hydraulic performance of a nanofluid flow through a tube. J Therm Anal Calorim. 2019;. https://doi.org/10.1007/s10973-019-08683-x.
17. Seyednezhad M, Sheikholeslami M, Ali JA, Shafee A, Nguyen TK. Nanoparticles for water desalination in solar heat exchanger. J Therm Anal Calorim. 2019;. https://doi.org/10.1007/s10973-019-08634-6.
18. Sheikholeslami M, Hayat T, Alsaedi A. MHD free convection of Al_2O_3-water nanofluid considering thermal radiation: a numerical study. Int J Heat Mass Transf. 2016;96:513–24.
19. Prasannakumara BC, Gireesha BJ, Krishnamurthy MR, Kumar KG. MHD flow and nonlinear radiative heat transfer of Sisko nanofluid over a nonlinear stretching sheet. Inf Med Unlocked. 2017;9:123–32.
20. Sheikholeslami M, Ellahi R. Three dimensional mesoscopic simulation of magnetic field effect on natural convection of nanofluid. Int J Heat Mass Transf. 2015;89:799–808.
21. Sajid M, Hayat T. The application of homotopy analysis method for MHD viscous flow due to a shrinking sheet, Chaos. Soli Frac. 2009;39:1317–23.
22. Hsiao KL. Stagnation electrical MHD nanofluid mixed convection with slip boundary on a stretching sheet. Appl Therm Eng. 2016;98:850–61.
23. Cortell R. MHD (magneto-hydrodynamic) flow and radiative nonlinear heat transfer of a viscoelastic fluid over a stretching sheet with heat generation/absorption. Energy. 2014;74:896–905.
24. Sheikholeslami M. Magnetic field influence on CuO-H_2O nanofluid convective flow in a permeable cavity considering various shapes for nanoparticles. Int J Hydr Energy. 2017;42:19611–21.
25. Sheikholeslami M. Solidification of NEPCM under the effect of magnetic field in a porous thermal energy storage enclosure using CuO nanoparticles. J Mol Liq. 2018;263:303–15.
26. Sheikholeslami M, Shehzad SA, Li Z, Shafee A. Numerical modeling for alumina nanofluid magnetohydrodynamic convective heat transfer in a permeable medium using Darcy law. Int J Heat Mass Transf. 2018;127:614–22.
27. Sheikholeslami M, Li Z, Shafee A. Lorentz forces effect on NEPCM heat transfer during solidification in a porous energy storage system. Int J Heat Mass Transf. 2018;127:665–74.
28. Sheikholeslami M. Numerical approach for MHD Al_2O_3 -water nanofluid transportation inside a permeable medium using innovative computer method. Comput Meth Appl Mech Eng. 2019;344:306–18.
29. Sheikholeslami M, Sheremet MA, Shafee A, Li Z. CVFEM approach for EHD flow of nanofluid through porous medium within a wavy chamber under the impacts of radiation and moving walls. J Therm Anal Calorim. 2019;138:573. https://doi.org/10.1007/s10973-019-08235-3.
30. Khan M, Munawar S, Abbasbandy S. Steady flow and heat transfer of a Sisko fluid in annular pipe. Int J Heat Mass Transf. 2010;53(7–8):1290–7.
31. Khan M, Shaheen N, Shahzad A. Steady flow and heat transfer of a magnetohydrodynamic Sisko fluid through porous medium in annular pipe. Int J Num Methods Fluids. 2012;69:1907–22.
32. Khan M, Shahzad A. On boundary layer flow of a Sisko fluid over a stretching sheet. Quaest Math. 2013;36:137–51.
33. Malik R, Khan M, Munir A, Khan WA. Flow and heat transfer in Sisko fluid with convective boundary condition. PLOS One. 2014;9:e107989.
34. Mahmood M, Asghar S, Hossain MA. Squeezed flow and heat transfer over a porous surface for viscous fluid. Int J Heat Mass Transf. 2007;44:165–73.
35. Salahuddin T, Malik MY, Hussain A, Bilal S, Awais M. Combined effects of variable thermal conductivity and MHD flow on pseudoplastic fluid over a stretching cylinder by using Keller box method. Inf Sci Lett. 2016;5:11–9.
36. Abel S, Prasad KV, Mahaboob A. Buoyancy force and thermal radiation effects in MHD boundary layer visco-elastic fluid flow over continuously moving stretching surface. Int J Therm Sci. 2005;44:465–76.
37. Malik MY, Hussain A, Salahuddin T, Awais M, Bilal S. Magnetohydrodynamic flow of Sisko fluid over a stretching cylinder

with variable thermal conductivity: a numerical study. AIP Adv. 2016;6(2):025316.
38. Malik MY, Bibi M, Khan F, Salahuddin T. Numerical solution of Williamson fluid flow past a stretching cylinder and heat transfer with variable thermal conductivity and heat generation/absorption. AIP Adv. 2016;6(3):035101.
39. Sui J, Zheng L, Zhang X, Chen G. Mixed convection heat transfer in power law fluids over a moving conveyor along an inclined plate. Int J Heat Mass Transf. 2015;85:1023–33.
40. Pal D, Chatterjee S. Soret and Dufour effects on MHD convective heat and mass transfer of a power-law fluid over an inclined plate with variable thermal conductivity in a porous medium. Appl Math Comput. 2013;219:7556–74.
41. Datti PS, Prasad KV, Abel MS, Joshi A. MHD visco-elastic fluid flow over a non-isothermal stretching sheet. Int J Eng Sci. 2004;42:935–46.
42. Zheng LC, Zhang XX, Lu CQ. Heat transfer for power law non-Newtonian fluids. Chin Phy Lett. 2006;23:3301.
43. Ellahi R, Hassan M, Zeeshan A. A study of heat transfer in power law nanofluid. Therm Sci. 2016;20(6):2015–26.
44. Hayat T, Anwar MS, Farooq M, Alsaedi A. Mixed convection flow of viscoelastic fluid by a stretching cylinder with heat transfer. PLOS One. 2015;10(3):e0118815.
45. Zhang C, Zheng L, Zhang X, Chen G. MHD flow and radiation heat transfer of nanofluids in porous media with variable surface heat flux and chemical reaction. Appl Math Model. 2015;39:165–81.
46. Yu W, Choi SUS. The role of interfacial layers in the enhanced thermal conductivity of nanofluids: a renovated Maxwell model. J Nanopart Res. 2003;5:167–71.
47. Koo J, Kleinstreuer C. A new thermal conductivity model for nanofluids. J Nanopart Res. 2004;6:577–88.
48. Das K. Slip flow and convective heat transfer of nanofluids over a permeable stretching surface. Comp Fluids. 2012;64:34–42.
49. Huang Z, Zhang W, Xi G. Natural convection in square enclosure induced by inner circular cylinder with time-periodic pulsating temperature. Int J Heat Mass Transf. 2015;82:16–25.
50. Bhowmick S, Molla MM, Mia M, Saha SC. Non-Newtonian mixed convection flow from a horizontal circular cylinder with uniform surface heat flux. Proc Eng. 2014;90:510–6.
51. Malik R, Khan M, Munir A, Khan WA. Flow and heat transfer in Sisko fluid with convective boundary condition. PLOS One. 2014;9(10):e107989.
52. Bhattacharyya K. Dual solutions in boundary layer stagnation-point flow and mass transfer with chemical reaction past a stretching/shrinking sheet. Int Commun Heat Mass Transf. 2011;38:917–22.
53. Ishak A, Lok YY, Pop I. Stagnation-point flow over a shrinking sheet in a micropolar fluid. Chem Eng Commun. 2010;197:1417–27.